

Synthesis of Hollow Ni_{0.75}Zn_{0.25}Fe₂O₄ Nanospheres and Their Sodium Storage Performance Post-print

Authors: Wei Hechun, Pang Hao, Li Huanjian, Dongliang Yan, Yan Dongliang

Date: 2022-10-26T00:00:00+00:00

Abstract

To investigate the electrochemical performance of ternary transition metal oxides as anode materials for sodium-ion batteries, hollow Ni_{0.75}Zn_{0.25}Fe₂O₄ nanospheres with a diameter of approximately 230 nm were successfully prepared via a hydrothermal method. The as-prepared hollow Ni_{0.75}Zn_{0.25}Fe₂O₄ nanospheres exhibit a high specific surface area of 32.6 m²/g and good dispersibility. When used as an anode material for sodium-ion batteries, the hollow Ni_{0.75}Zn_{0.25}Fe₂O₄ nanospheres demonstrate excellent cycle life and rate capability: after 800 cycles at a current density of 200 mA/g, a specific discharge capacity of 178.5 mA · h/g is retained, with a high capacity retention of 91.6%; after 800 cycles at a current density of 500 mA/g, the capacity retention is 89.3%. Furthermore, at current densities of 100, 200, 500, 1,000, and 2,000 mA/g, the average specific discharge capacities are 212.7, 191.4, 148, 121.8, and 100 mA · h/g, respectively. The excellent electrochemical performance of the hollow Ni_{0.75}Zn_{0.25}Fe₂O₄ nanosphere electrode can be attributed to its unique nanohollow structure, high specific surface area, and shortened electron and ion transport pathways, which improves its electrochemical performance during the Na⁺ insertion/extraction process.

Full Text

Synthesis and Sodium Storage Performance of Ni_{0.75}Zn_{0.25}Fe₂O₄ Hollow Nanospheres

Hechun Wei¹, Huanjian Li¹, Dongliang [Last Name Missing]¹

¹School of Materials Science and Engineering, Guangxi Key Laboratory of Information Materials, Guilin University of Electronic Technology, Guilin 541004, China

Abstract

To investigate the electrochemical performance of ternary transition metal oxides as anode materials for sodium-ion batteries, hollow Ni_{0.75}Zn_{0.25}Fe₂O₄ nanospheres were successfully synthesized via a hydrothermal method. The prepared hollow nanospheres exhibit high specific surface area and good dispersibility. When employed as a sodium-ion battery anode, the material demonstrates excellent cycling stability and rate capability. At a current density of [value] mA/g, the electrode maintains a discharge specific capacity of [value] mA · h/g after [number] cycles, with a capacity retention of 91.6%. The average discharge specific capacities at current densities of 100, 200, 500, and 1000 mA/g are 212.7, 191.4, 148, and 121.8 mA · h/g, respectively. The superior electrochemical performance can be attributed to the unique hollow nanostructure, which shortens electron and ion transport pathways and enhances electrochemical kinetics during sodium insertion/extraction processes.

Keywords: Ni_{0.75}Zn_{0.25}Fe₂O₄; sodium-ion battery; anode material; hollow nanospheres

Introduction

Sodium-ion batteries (SIBs) have emerged as the most promising alternative to lithium-ion batteries (LIBs) due to the natural abundance and low cost of sodium resources, coupled with the similar physicochemical properties of sodium and lithium. However, the larger ionic radius of Na⁺ (0.102 nm) compared to Li⁺ (0.076 nm) poses significant challenges for electrode materials, as it impedes ion diffusion and causes substantial volume expansion during cycling. Among various anode materials under investigation, transition metal oxides have attracted considerable attention because of their high theoretical capacities. Within this family, iron-based oxides are particularly promising for SIBs due to their low toxicity, environmental benignity, and theoretical specific capacities ranging from 720 to 900 mA · h/g.

Zinc-nickel ferrite (Ni_{0.75}Zn_{0.25}Fe₂O₄) has garnered increased interest because the complementary and synergistic effects of nickel and zinc enhance electronic and ionic conductivity, thereby improving electrochemical performance. Nevertheless, like many transition metal oxide anodes, it suffers from rapid capacity fading and poor rate performance. To address these issues, rational design of nanostructured materials with special morphologies has proven effective. Hollow nanosphere architectures are especially advantageous as they provide abundant electrochemical reaction active sites, shorten ion diffusion distances, accommodate volume expansion, and facilitate electrolyte penetration, ultimately delivering superior rate capability and cycling stability.

This work presents a facile hydrothermal synthesis of hollow Ni_{0.75}Zn_{0.25}Fe₂O₄ nanospheres and evaluates their performance as SIB anode materials. The

unique structural features and their correlation with electrochemical properties are systematically investigated.

Experimental Methods

Materials Synthesis

Hollow Ni_{0.75}Zn_{0.25}Fe₂O₄ nanospheres were prepared via a simple hydrothermal method followed by thermal annealing. Stoichiometric amounts of Ni(NO₃)₂ · 6H₂O, Zn(NO₃)₂ · 6H₂O, and Fe(NO₃)₃ · 9H₂O were dissolved in ethylene glycol containing polyvinylpyrrolidone (PVP) as a surfactant. The mixture was magnetically stirred to obtain a homogeneous solution, which was then transferred to a stainless steel autoclave and subjected to hydrothermal treatment at [temperature] for [duration]. After cooling, the precursor was collected by centrifugation, thoroughly washed with deionized water and ethanol, and dried. Finally, the precursor powder was calcined in a muffle furnace at [temperature] to obtain the hollow Ni_{0.75}Zn_{0.25}Fe₂O₄ nanospheres.

Characterization

The crystal structure of the product was characterized by X-ray diffraction (XRD, D8-Advance, Bruker). Morphology and microstructure were examined using field emission scanning electron microscopy (FESEM, Tecnai-450) and transmission electron microscopy (TEM, Talos F200X). The specific surface area and pore size distribution were determined by nitrogen adsorption-desorption measurements (ASAP 2020, Micromeritics) using the Brunauer-Emmett-Teller (BET) and Barrett-Joyner-Halenda (BJH) methods. The elemental composition and chemical states were analyzed by X-ray photoelectron spectroscopy (XPS, Escalab 250Xi, Thermo Fisher).

Electrochemical Measurements

The working electrode was prepared by mixing the active material, conductive carbon, and sodium carboxymethyl cellulose (CMC) binder in a mass ratio of 7:2:1 with an appropriate amount of deionized water. The slurry was ground in a mortar and uniformly coated onto copper foil, followed by vacuum drying at [temperature]. CR2032 coin cells were assembled in an argon-filled glove box using metallic sodium as the counter electrode, Whatman glass fiber as the separator, and 1 mol/L NaClO₄ in EC/DEC as the electrolyte. Galvanostatic charge-discharge tests were conducted on a Land battery testing system within a voltage window of 0.01–3.0 V (vs. Na⁺/Na). Cyclic voltammetry (CV) was performed on a CHI660E electrochemical workstation at a scan rate of 0.1 mV/s.

Results and Discussion

Structural and Morphological Characterization

The XRD pattern of the prepared Ni_{0.75}Zn_{0.25}Fe₂O₄ hollow nanospheres is shown in [FIGURE:N]. All diffraction peaks at 18.4°, 30.1°, 35.5°, 37.2°, 43.2°, 53.3°, 57.2°, and 62.8° can be indexed to the (111), (220), (311), (222), (400), (422), (511), and (440) crystal planes of spinel Ni_{0.75}Zn_{0.25}Fe₂O₄ (JCPDS No. 52-0277), respectively. The absence of any impurity peaks confirms the high phase purity of the product.

Scanning electron microscopy images reveal that the Ni_{0.75}Zn_{0.25}Fe₂O₄ sample consists of uniform spherical particles with an average diameter of approximately [value] nm [FIGURE:N]. The nanospheres exhibit excellent dispersibility without apparent aggregation, which is crucial for maintaining stable electrochemical performance. Transmission electron microscopy analysis further confirms the hollow interior structure of the nanospheres [FIGURE:N]. This hollow architecture increases the electrode-electrolyte contact area and provides ample space to accommodate volume changes during sodiation/desodiation, thereby enhancing cycling stability.

Nitrogen adsorption-desorption isotherms display typical type-IV characteristics with a distinct hysteresis loop, confirming the presence of mesopores [FIGURE:N]. The BET specific surface area is calculated to be [value] m²/g, and the average pore size is [value] nm according to the BJH method. The high specific surface area provides more active sites for electrochemical reactions and facilitates ion transport, contributing to the superior performance.

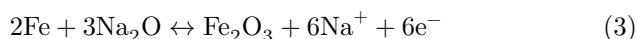
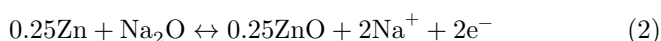
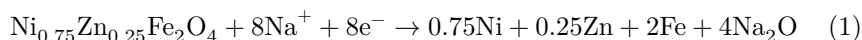
X-ray photoelectron spectroscopy was employed to determine the surface elemental composition and oxidation states. The Fe 2p spectrum exhibits two prominent peaks at 710.8 eV and 724.9 eV, corresponding to Fe 2p_{3/2} and Fe 2p_{1/2}, respectively, which are characteristic of Fe³⁺. Satellite peaks appear at 719.5 eV. The Ni 2p spectrum shows binding energies at 856.2 eV and 872.8 eV for Ni 2p_{3/2} and Ni 2p_{1/2}, with satellite peaks at 862.3 eV and 876.7 eV, consistent with Ni²⁺. The Zn 2p spectrum displays peaks at 1021.4 eV and 1044.7 eV, confirming Zn²⁺. The O 1s spectrum reveals two components: a peak at 529.8 eV attributed to metal-oxygen bonds and another at 531.5 eV corresponding to lattice oxygen.

Electrochemical Performance

The cyclic voltammetry curves of the Ni_{0.75}Zn_{0.25}Fe₂O₄ hollow nanosphere electrode at a scan rate of 0.1 mV/s in the voltage range of 0.01–3.0 V are presented in [FIGURE:N]. In the first cathodic scan, a pronounced reduction peak appears at approximately [voltage] V, corresponding to the reduction of Ni²⁺, Zn²⁺, and Fe³⁺ to metallic Ni, Zn, and Fe, respectively, along with the formation of a solid electrolyte interphase (SEI) layer. This peak shifts to a higher potential in subsequent cycles, indicating an irreversible phase transformation

during the initial sodiation process. In the anodic scan, strong oxidation peaks observed at [voltage] V are attributed to the oxidation of Zn, Ni, and Fe to ZnO, NiO, and Fe₂O₃, respectively. The nearly overlapping CV curves from the second cycle onward demonstrate excellent reversibility and structural stability of the electrode.

The overall sodiation/desodiation mechanism can be expressed by the following equations:



Galvanostatic charge-discharge curves at a current density of [value] mA/g are shown in [FIGURE:N]. The initial discharge and charge capacities are 341.1 and 176.2 mA · h/g, respectively, yielding a Coulombic efficiency of 51.7%. The irreversible capacity loss in the first cycle is primarily attributed to electrolyte decomposition and SEI film formation. In the second cycle, the discharge and charge capacities are 194.8 and 173.2 mA · h/g, respectively, with the Coulombic efficiency increasing to 88.9%. From the third cycle onward, the Coulombic efficiency remains near 100%, indicating excellent reversibility.

The cycling performance of the Ni_{0.75}Zn_{0.25}Fe₂O₄ hollow nanosphere electrode is presented in [FIGURE:N]. At a current density of [value] mA/g, the electrode delivers a discharge capacity of [value] mA · h/g after [number] cycles, corresponding to a capacity retention of 91.6% relative to the second cycle. Even at a higher current density of [value] mA/g, the electrode maintains [value] mA · h/g after [number] cycles with 89.3% capacity retention. These results surpass previously reported values for similar materials, demonstrating the superior cycling stability of the hollow nanosphere architecture.

Rate capability tests further highlight the advantages of the hollow structure. As shown in [FIGURE:N], the electrode achieves average discharge capacities of 212.7, 191.4, 148, and 121.8 mA · h/g at current densities of 100, 200, 500, and 1000 mA/g, respectively. When the current density is reduced back to [value] mA/g, the discharge capacity recovers to [value] mA · h/g, confirming the robustness of the electrode structure under varying operating conditions. This rate performance compares favorably with literature reports [9-10,14].

Conclusion

In summary, hollow Ni_{0.75}Zn_{0.25}Fe₂O₄ nanospheres with good dispersibility have been successfully synthesized via a facile hydrothermal method. When evaluated as an anode material for sodium-ion batteries, the material exhibits excel-

lent electrochemical performance, including high specific capacity, outstanding cycling stability (91.6% and 89.3% retention under different conditions), and superior rate capability. The enhanced performance is primarily attributed to the unique hollow nanostructure, which provides a high specific surface area, shortens electron and ion diffusion pathways, accommodates volume expansion during cycling, and improves electrode-electrolyte contact. This simple synthesis strategy offers a promising approach for designing other unary or multinary transition metal oxide nanostructures for advanced energy storage applications beyond batteries, including supercapacitors and other electrochemical devices.

References

- [1] SLATER D, KIM H, LEE J, et al. Sodium-ion batteries[J]. *Advanced Functional Materials*, 2013, 23(8): 947-958.
- [2] LIU H, JIA M, SUN N, et al. Nitrogen-rich mesoporous carbon as high-performance anode material for sodium-ion batteries[J]. *ACS Applied Materials & Interfaces*, 2015, 7(49): 27124-27130.
- [3] FANG Y, YU X, LOU X. Formation of Cu-doped CoSe_2 microboxes via sequential ion exchange for high-performance sodium-ion batteries[J]. *Advanced Materials*, 2018, 30(21): [page numbers].
- [4] LI Y, WANG Z, LI L, et al. Preparation of nitrogen- and phosphorous co-doped carbon for sodium-ion batteries[J]. *ACS Applied Materials & Interfaces*, 2018, 10(39): 33170-33178.
- [5] FANG Y, XIAO L, CHEN Z, et al. Recent advances in sodium-ion battery materials[J]. *Electrochemical Energy Reviews*, 2018, 1(3): 294-323.
- [6] ZHANG J, CHEN T, YAN X, et al. MgFe_2O_4 /reduced graphene oxide composites as high-performance anode materials for sodium-ion batteries[J]. *Electrochimica Acta*, 2015, 180: 616-621.
- [7] REDDY V, QUAN Y, TEO S, et al. Mixed metal ferrites ($\text{Ni}_x\text{Zn}_{1-x}\text{Fe}_2\text{O}_4$, $x = 0, 0.25, 0.5, 0.75, 1$): synthesis, characterization, and lithium storage performance[J]. *The Journal of Physical Chemistry C*, 2015, 119(9): 4709-4719.
- [8] MAO J, HOU X, HUANG F, et al. Enhanced conductivity of NiFe_2O_4 nanoparticles for high-performance lithium battery electrodes[J]. *Journal of Alloys and Compounds*, 2016, 676: 265-274.
- [9] WU F, WANG X, LI M, et al. NiFe_2O_4 /RGO nanocomposites as superior anode materials for lithium-ion batteries[J]. *Ceramics International*, 2016, 42(15): 16666-16670.
- [10] ZHOU K, KANG M, HE X, et al. Multi-functional arabic gum binder enabling molten NiFe_2O_4 nanotube anodes with excellent Li/Na-ion storage performance[J]. *Journal of Materials Chemistry A*, 2017, 5(34): 18138-18147.

- [11] CHERIAN T, REDDY V, RAO B, et al. Li-storage properties of nanocrystalline $(\text{Ni}_{1-x}\text{Zn}_x)\text{Fe}_2\text{O}_4$ ($0 \leq x \leq 1$)[J]. *Journal of Solid State Electrochemistry*, 2012, 16(5): 1823-1832.
- [12] LI L, JIN B, LANG J, et al. ZnFe_2O_4 lithium storage materials[J]. *ChemPlusChem*, 2016, 81(11): 1174-1181.
- [13] LUO X, ZHANG X, CHEN L, et al. Facile synthesis of mesoporous ZnMn_2O_4 microtubules derived from a morphological transformation strategy for high-performance lithium/sodium storage[J]. *Journal of Materials Chemistry A*, 2015, 3(26): 13807-13818.
- [14] GUO C, LIU J, YANG Y, et al. Mg- Fe_2O_4 hollow microboxes derived from metal-organic frameworks as anode material for sodium-ion batteries[J]. *Materials Letters*, 2017, 199: 101-104.
- [15] LIU J, YUAN Y, ZHU Z, et al. Three-dimensionally interconnected nickel-antimony intermetallic hollow nanospheres as high-rate anode material for sodium-ion batteries[J]. *Nano Energy*, 2015, 16: 389-398.
- [16] YU M, HUANG Y, WANG K, et al. ZnFe_2O_4 hollow nanospheres with complete internal space utilization for lithium battery anodes[J]. *Applied Surface Science*, 2018, 462: 955-962.
- [17] ZHANG C, TENG G, JIN C, et al. Controllable synthesis of hollow MnFe_2O_4 via self-etching for high-performance lithium-ion battery anodes[J]. *Chemical Engineering Journal*, 2019, 365: 121-131.
- [18] LI D, LI G, GE H, et al. Fabrication of nanoporous CoFe_2O_4 and NiFe_2O_4 spheres as promising anodes for lithium-ion batteries[J]. *New Journal of Chemistry*, 2017, 41(24): 15501-15508.
- [19] KIM G, KIM M, NOH J, et al. Formation of carbon-coated ZnFe_2O_4 nanowires with highly reversible lithium storage properties[J]. *RSC Advances*, 2014, 4(53): 27714-27721.
- [20] ZHOU S, LUO X, CHEN L, et al. MnCo_2O_4 nanospheres with improved sodium storage performance[J]. *Ceramics International*, 2018, 44(15): [page numbers].
- [21] LI Y, MENG Y, LIU X, et al. Double-protected ferrite nanospheres as stable anode materials for lithium batteries[J]. *Journal of Power Sources*, 2019, 442: 227256-227264.
- [22] FU Y, WEI Q, WANG X, et al. Hollow $\alpha\text{-Fe}_2\text{O}_3@ \text{TiO}_2$ core-shell nanospheres for lithium storage[J]. *Journal of Materials Chemistry A*, 2016, 4(39): [page numbers].
- [23] PEI T, STEVIN S, YOGESH S, et al. Electrospun Fe_3O_4 nanofibers as anodes for lithium-ion batteries: impact of mixed metallic oxides on performance[J]. *ACS Applied Materials & Interfaces*, 2013, 5(12): 5461-5467.

Editor: Zhang Suobin

Note: Figure translations are in progress. See original paper for figures.

Source: ChinaXiv – Machine translation. Verify with original.